ACS APPLIED MATERIALS & INTERFACES

Research Article

www.acsami.org

Construction of ZnO/ZnS/CdS/$CuInS_2$ Core–Shell Nanowire Arrays via Ion Exchange: p–n Junction Photoanode with Enhanced Photoelectrochemical Activity under Visible Light

Yu-Xiang Yu,* Wei-Xin Ouyang, Zhou-Ting Liao, Bin-Bin Du, and Wei-De Zhang*

School of Chemistry and Chemical Engineering, South China University of Technology, 381 Wushan Road, Guangzhou 510640, People's Republic of China

Supporting Information

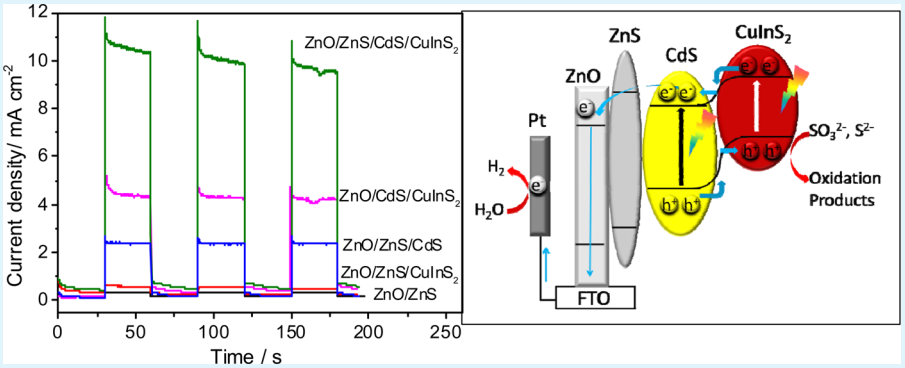

ABSTRACT: ZnO/ZnS/CdS/$CuInS_2$ core–shell nanowire arrays with enhanced photoelectrochemical activity under visible light were successfully prepared via ion exchange and hydrothermal methods. The samples were characterized by X-ray diffraction, scanning electron microscopy, transmission electron microscopy, UV–vis absorption, X-ray photoemission spectroscopy, and photoelectrochemical response. As a p–n junction photoanode, ZnO/ZnS/CdS/$CuInS_2$ heterostructure shows much higher visible light photoelectrocatalytic activity toward water splitting than ZnO/ZnS/CdS and ZnO/ZnS films. The ZnO/ZnS/CdS/$CuInS_2$ film with optimal constitution exhibits the highest photocurrent of 10.5 mA/cm^2 and the highest IPCE of approximately 57.7% at 480 nm and a bias potential of 0 V versus Ag/AgCl. The critical roles of CdS and ZnS in ZnO/ZnS/CdS/$CuInS_2$ heterostructure were investigated. ZnS, as a passivation layer, suppresses the recombination of the photogenerated charge carriers at the interface of the oxide and $CuInS_2$. CdS enhances the absorption of visible light and forms p–n junctions with $CuInS_2$, which promotes the transport of charge carriers and retards the recombination of electrons and holes in $CuInS_2$ to improve the photoelectrochemical performance of ZnO/ZnS/CdS/$CuInS_2$ heterostructure.

KEYWORDS: *ZnO/ZnS/CdS/$CuInS_2$, core–shell, p–n junction, photoelectrochemical property*

INTRODUCTION

Solar energy, as a kind of inexhaustible and clean energy, holds great potential to cope with the world energy crisis and to solve energy-related environmental problems. However, how to utilize sunlight effectively and economically in usable energy forms remains a great technical challenge. Photoelectrochemical water splitting is accepted as a promising way to convert solar energy to zero-emission and renewable hydrogen fuel with high energy density. Continuous efforts have been made to construct highly-efficient and stable photoelectrochemical systems.[1−9] Effective electron percolation pathways, high surface-to-volume ratio, and improved light scattering ability for light harvesting have made the perpendicularly-aligned and highly-ordered ZnO nanowire arrays an excellent candidate for a photoelectrochemical photoanode. However, a number of unfavorable issues, such as the short lifetime of the charge carriers and its sole absorption of UV light, limit the photoelectrochemical efficiency of ZnO nanowire arrays.[10−12] In order to remedy these defects, specific semiconductors have been coated or randomly decorated on the surface of ZnO nanowires to extend visible light absorption and to build heterojunctions with ZnO to facilitate the separation and transportation of photogenerated charge carriers so as to improve the kinetics of water-splitting processes.[13−16]

Copper indium disulfide ($CuInS_2$), free of toxic elements, is an ideal semiconductor for capturing the sunlight owing to its high absorption coefficient of 10^5 cm^{-1} and direct bandgap (E_g) of 1.53 eV which is well-matched with the solar spectrum.[17−19] Moreover, $CuInS_2$ exhibits intrinsic p-type semiconductive behavior when the atomic ratio of Cu to In exceeds 1.[20]

Received: March 6, 2014
Accepted: April 23, 2014
Published: April 23, 2014

$CuInS_2$-based p−n junctions are expected to be high-performance photoelectrodes, because the p−n junction causes the space charge region at the junction where electrons are depleted and an internal electrostatic field is established. The internal electric field forces electrons and holes to diffuse to opposite directions, thus reducing their recombination.[21−24] Although several $CuInS_2$-based p−n heterojunctions have been reported,[15,25,26] such as $ZnO/CuInS_2$[15] and $TiO_2/CuInS_2$,[25] it remains a technical challenge to obtain high quality $CuInS_2$-based p−n heterojunctions with completely conformal surface coverage of nanowire arrays. Defects of contact and uniformity will inevitably emerge when quantum dots are simply deposited on nanowire arrays by dip-coating or spin-coating. Recently, $ZnO/CuInS_2$ core/shell nanorods were prepared by hydrothermal and cation exchange methods, by which uniform $CuInS_2$ films were obtained on the surface of ZnO nanorods and improved efficiency of photoelectrochemical water splitting was achieved.[15] However, when a wide bandgap semiconductor, such as TiO_2, was directly sensitized with $CuInS_2$ for quantum-dot-sensitized solar cells, it displayed mismatched band alignments and high surface state density in the heterostructure between TiO_2 and $CuInS_2$. As a result, the charge separation at such heterostructure interfaces is poor.[27] It also exhibited slow hole scavenging and prompt electron−hole recombination between $CuInS_2$ and electrolytes.[28] CdS and ZnS, as buffer layer and passivation layer, respectively, were believed to retard recombination of charge carriers at the $TiO_2/CuInS_2$/electrolyte interfaces and to enhance the photovoltaic performance.[29−31] Teng and his colleagues reported that the CdS coating improved the photoelectrochemical performance of $TiO_2/CuInS_2$ electrodes by extending the absorption spectra of the $CuInS_2$ and facilitating charge separation by scavenging photogenerated holes in the valence band of the $CuInS_2$.[32]

To the best of our knowledge, the roles of CdS and ZnS in $ZnO/CuInS_2$ heterostructures for photoelectrochemical water splitting have not been fully investigated. In this study, $ZnO/ZnS/CdS/CuInS_2$ core−shell nanowire arrays were prepared by ion exchange and hydrothermal processes. Ion exchange has been demonstrated as an effective way to alter the chemical compositions of nanostructures without destroying the original morphology and to ensure the formation of high quality heterojunctions. The $ZnO/ZnS/CdS/CuInS_2$ heterostructure shows much higher visible light photoelectrocatalytic activity toward water splitting than ZnO/ZnS/CdS and ZnO/ZnS films. CdS and ZnS play critical roles in the improvement of photoelectrochemical performance of the composite electrode. It demonstrates a new approach to build highly efficient photoanodes in photoelectrochemical water splitting.

EXPERIMENTAL SECTION

Materials. $Zn(CH_3COO)_2{\cdot}2H_2O$, $Cu(NO_3)_2{\cdot}3H_2O$, and $Na_2S{\cdot}9H_2O$ were purchased from Guangzhou Chemical Reagent Factory, whereas $Cd(NO_3)_2{\cdot}4H_2O$ and Na_2SO_3 were from Kermel Chemical Reagent Company (Tianjin, China). Thioacetamide (TAA) and triethylene glycol (TEG) were bought from Shanghai Lingfeng Chemical Reagent Company. $In(NO_3)_3{\cdot}4.5H_2O$ and hexamethylenetetramine ($C_6H_{12}N_4$) were obtained from Sinopharm Chemical Reagent Company and Chengdu Union Chemical Industry Reagent Institute, respectively. All chemicals were of analytical grade and used without further purification. Deionized water (resistivity >18.4 MΩ/cm) was from a pure water system (GWA-UN). Fluorine-doped tin oxide (FTO)-coated glass was purchased from Nippon Sheet Glass Company, Japan. FTO-coated glass was sliced to be 30 mm × 10 mm per piece, and the FTO pieces were then successively sonicated in acetone and ethanol and then rinsed with deionized water.

Preparation of $ZnO/ZnS/CdS/CuInS_2$ Nanowire Arrays. Preparation of ZnO nanowire arrays was described elsewhere.[12,33] Typically, FTO was firstly soaked with 5 mmol/L ethanol solution of zinc acetate to form the seed layer. The dense layer was annealed at 350 °C for 30 min to form the ZnO nanocrystalline layer. Nanowire arrays were grown by immersing seeded substrates in an aqueous solution containing 25 mmol/L zinc nitrate hydrate, 25 mmol/L hexamethylenetetramine, and 6 mmol/L polyethylenimine (branched, low molecular weight, Aldrich) at 95 °C for 3 h. The as-grown ZnO nanowire arrays were further annealed in air at 400 °C for 60 min to improve the crystallinity of the nanowires and decrease the interfacial defects.

$ZnO/ZnS/CdS/CuInS_2$ core−shell nanowires were constructed by a series of ion exchange and hydrothermal processes. Firstly, the as-prepared ZnO nanowire arrays reacted with 0.20 mol/L TAA solution at 90 °C for 6 h to prepare ZnO/ZnS nanowire arrays. Secondly, the ZnO/ZnS nanowire arrays were put in a Telfon-lined stainless autoclave, which contained a 0.10 mol/L $Cd(NO_3)_2$ aqueous solution, and maintained at 95 °C for 3 h to fabricate ZnO/ZnS/CdS nanowire arrays. ZnS could be totally replaced by CdS, resulting in ZnO/CdS nanowire arrays, with extending the reaction time and using a higher concentration of $Cd(NO_3)_2$ solution. To prepare $ZnO/ZnS/CuInS_2$, $ZnO/CdS/CuInS_2$, and $ZnO/ZnS/CdS/CuInS_2$, the ZnO/ZnS, ZnO/CdS, and ZnO/ZnS/CdS nanowire arrays were immersed, respectively, in 2.5 mmol/L $Cu(NO_3)_2$ aqueous solution at 75 °C for 10 s and then put in Teflon-lined stainless autoclaves, all filled with 40 mL of TEG solution containing 0.060 mmol $In(NO_3)_3{\cdot}4.5H_2O$. The autoclaves were then sealed and maintained at 200 °C for 3 h. Lastly, the samples were washed with deionized water and dried at 90 °C.

Characterization. The morphology of the samples was characterized by scanning electron microscopy (SEM, Philips CM 300FE) and transmission electron microscopy (TEM, Tecnai G220, FEI). X-ray diffraction (XRD) patterns were recorded on an X'Pert MPD Pro X-ray diffractometer using Cu Kα radiation. UV−vis spectroscopy was conducted on a Hitachi U3010 spectrophotometer using $BaSO_4$ as a reference.

Electrochemical Measurements. Typically, a three-electrode configuration in a quartz cell was assembled to test the photoelectrochemical activity of the samples on Chenghua electrochemical workstation (CHI660C, Shanghai). A Pt plate and a commercially available Ag/AgCl electrode were used as the counter and reference electrodes, and the prepared samples were employed as working electrodes. The effective surface area of the working electrode is 0.60 × 0.60 cm^2. All measured potential values are against Ag/AgCl reference electrode, unless otherwise indicated. The electrolyte used in all measurements was an aqueous solution containing 0.50 mol/L Na_2S and 0.50 mol/L Na_2SO_3. A 300 W xenon lamp (PLS-SXE300/300UV) equipped with a UV-light cut-off filter (λ > 420 nm) was used as visible light irradiation source. The output (visible light) intensity of the xenon lamp is about 150 mW/cm^2. The linear sweep voltammograms were operated at 100 mV/s in a potential range from −1.3 to +0.5 V versus Ag/AgCl both in dark and under illumination. The chronoamperometry curves of the films were obtained at 0 V versus Ag/AgCl. Electrochemical impedance spectroscopy (EIS) was performed under illumination with an AC amplitude of 10 mV and frequency range between 100 kHz and 1 Hz. A 500 W Xe lamp (CHF-XM-500, Changtuo Technology Co., Ltd.) and a monochromator (monochromator 300, Changtuo Technology Co., Ltd.) were used to measure wavelength-dependent photocurrents of all samples. The monochromatic light intensity was measured with a radiometer (PM120VA, Thorlabs). The incident photon to electron conversion efficiency (IPCE) of the samples was calculated as follows:

$$\mathrm{IPCE} = 1240 I(\mathrm{mA/cm^2})/[\lambda(\mathrm{nm}) J_{\mathrm{light}}(\mathrm{mW/cm^2})]$$

where I is the photocurrent density, λ is the wavelength of the monochromatic light, and J_{light} is the monochromatic light intensity.

Scheme 1. Preparation Process of the Core−Shell Heterojunctions

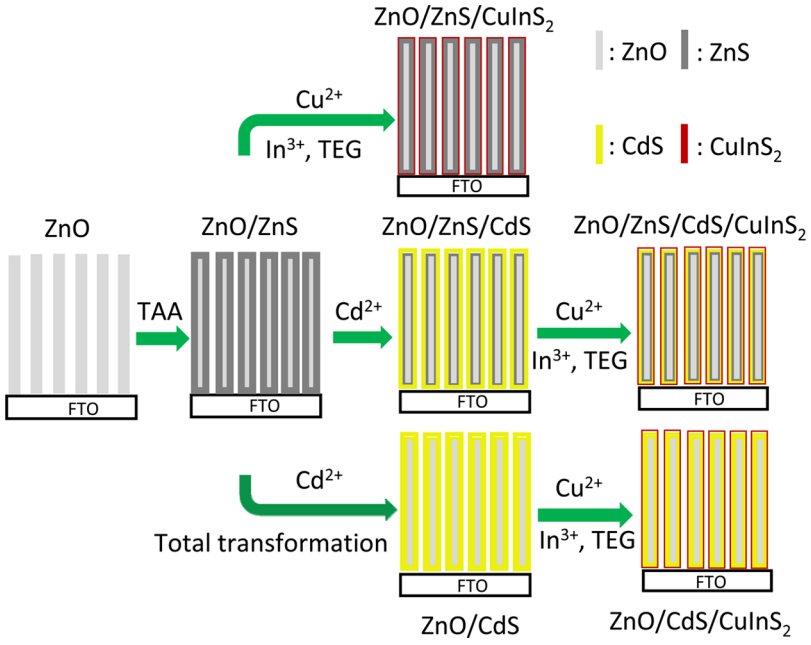

RESULTS AND DISCUSSION

XRD Patterns. ZnO nanowire arrays were firstly grown on FTO by a hydrothermal process. As illustrated in Scheme 1, the ZnO nanowire arrays were successively immersed in TAA, $Cd(NO_3)_2$, and $Cu(NO_3)_2$ aqueous solutions. In such processes, ZnO would partially or totally convert to ZnS, CdS, then to CuS by altering the solution concentration, reaction time, and reaction temperature due to the differences in solubility of the products ($K_{sp}(ZnO) = 6.8 \times 10^{-17}$, $K_{sp}(ZnS) = 2.93 \times 10^{-25}$, $K_{sp}(CdS) = 8.0 \times 10^{-27}$, $K_{sp}(CuS) = 1.27 \times 10^{-36}$).[15] Lastly, $ZnO/ZnS/CuInS_2$, $ZnO/CdS/CuInS_2$, and $ZnO/ZnS/CdS/CuInS_2$ core−shell nanoarrays were obtained through a polyol reduction reaction in TEG solution containing In^{3+}.

XRD patterns of all samples are shown in Figure 1. The diffraction peaks of Figure 1A can be well-indexed to the hexagonal phase ZnO (JCPDS 65-3411). After immersing in 0.20 mol/L TAA solution, ZnO reacts with S^{2-}, which is released from TAA at 90 °C at the surface of nanowires to form the ZnS layer. A new widened peak appears at 2θ of 28.6°, which is indexed to the cubic phase ZnS (JCPDS 05-0566) (Figure 1B). Further ion exchange and hydrothermal processes result in the formation of cubic phase CdS (JCPDS 10-0454) (Figure 1C) and tetragonal phase $CuInS_2$ (JCPDS 47-1372) (Figure 1D). The weak peak at 27.9° corresponding to $CuInS_2$ is due to the short reaction time with Cu^{2+}. The wide peaks at 26.5° (CdS) and 28.6° (ZnS) reveal that the newly generated ZnS and CdS layers are composed of very small crystals.

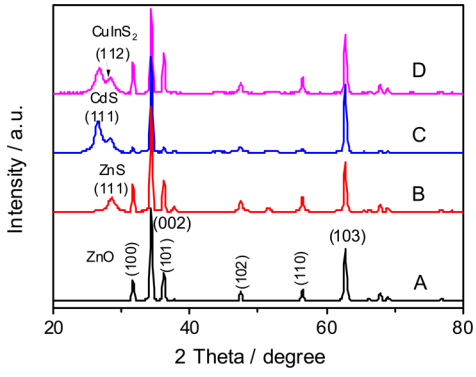

Figure 1. XRD patterns of (A) ZnO, (B) ZnO/ZnS, (C) ZnO/ZnS/CdS, and (D) $ZnO/ZnS/CdS/CuInS_2$ nanowire arrays.

SEM and TEM Images. Figure 2 shows the typical top-view SEM images of the bare and modified nanowire arrays grown on FTO. From Figure 2A, one can see that the nanowires with diameters of about 50−150 nm are perpendicularly aligned, with regular hexagonal tips. The lateral surfaces of the nanowires are angular and even, whereas the surfaces of the top are flat (inset in Figure 2A). Figure 2B−D show the top-view images of ZnO/ZnS, ZnO/ZnS/CdS, and $ZnO/ZnS/CdS/CuInS_2$ nanowire arrays, respectively. It is clearly demonstrated that the surfaces of the nanowires gradually grew rougher and bigger, indicating that the ion exchange reactions were achieved and new phases were formed. The EDX analysis of the final products demonstrates that Zn, Cd, Cu, In, S, and O elements co-exist and $ZnO/ZnS/CdS/CuInS_2$ nanowire array was successfully prepared (Figure 2E). Among all these elements, the atomic ratio of Cu to In is about 3:2, which exceeds 1. It reveals that $CuInS_2$ prepared in this way is a Cu-rich semiconductor and exhibits p-type behavior. To confirm the formation of $ZnO/ZnS/CdS/CuInS_2$ core−shell structure, the final product was observed by TEM (Figure 3) and elemental mapping (Figure S1, Supporting Information). From Figure 3A, one can see that the inner core of the nanowire is a monocrystal with irregular surface, and the outer layer consists of many closely-packed but randomly-oriented nanoparticles with a thickness 5−15 nm. The inner core with unitary lattice fringes is a single-crystal structure, and the fringe spacing of 0.26 nm corresponds to the (002) plane of wurtzite-type ZnO (inset of Figure 3A). The outer layer from the surface to the inside is made up of different crystal phases, and the fringe spacings of 0.32, 0.34, and 0.31 nm match well with the interplanar spacings of the (112) plane of $CuInS_2$, (111) plane

dx.doi.org/10.1021/am501336u | ACS Appl. Mater. Interfaces 2014, 6, 8467−8474

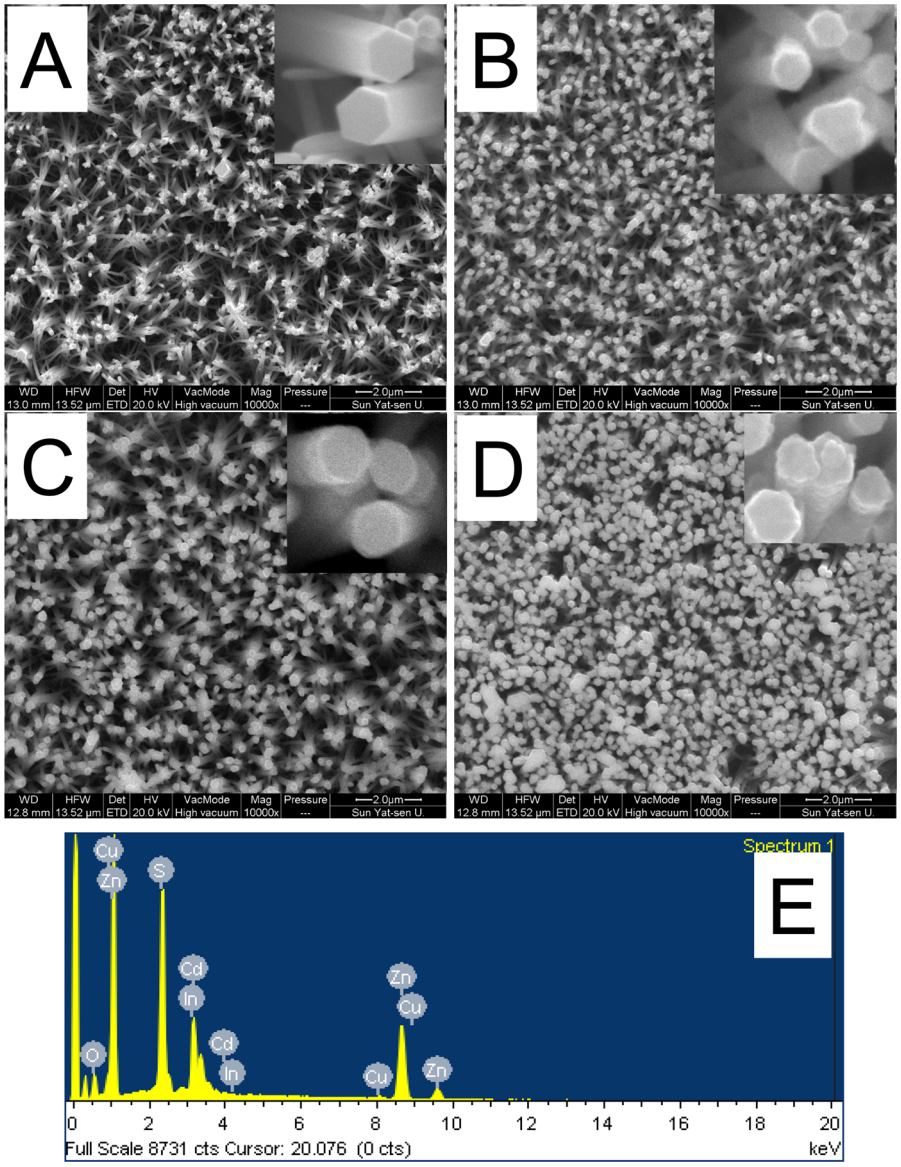

Figure 2. SEM images of (A) ZnO, (B) ZnO/ZnS, (C) ZnO/ZnS/CdS, and (D) ZnO/ZnS/CdS/$CuInS_2$ nanowire arrays. Insets are the corresponding high resolution images. (E) EDS analysis of ZnO/ZnS/CdS/$CuInS_2$.

of CdS, and (111) plane of ZnS crystals, respectively (Figure 3B). XPS analysis (Figure S2, Supporting Information) also proves the existence of ZnO, ZnS, CdS, and $CuInS_2$.

UV–vis Spectroscopy. The UV–vis diffuse reflectance spectra and optical images of ZnO, ZnO/ZnS, ZnO/ZnS/CdS, and ZnO/ZnS/CdS/$CuInS_2$ nanowire arrays were displayed in Figure 4. ZnO and ZnO/ZnS nanowire arrays are white and show almost no absorption in the visible light range. The absorption edges are all about 400 nm. After being ion-exchanged with Cd^{2+}, the sample turns yellow and absorbs part of the visible light. The absorption edge of ZnO/ZnS/CdS shifts to 530 nm, corresponding to the narrow bandgap (2.4 eV) of CdS. After ion-exchange with Cu^{2+} followed by a polyol reduction, the finally obtained sample, ZnO/ZnS/CdS/$CuInS_2$, becomes brown. Its absorption extends to a longer wavelength up to 700 nm and demonstrates prominent absorption in the visible light region due to the formation of $CuInS_2$ (bandgap of 1.53 eV). In sum, as direct narrow bandgap semiconductors, CdS can capture a considerable proportion of visible light, whereas $CuInS_2$ with a high absorption coefficient and proper bandgap can absorb and utilize even a larger proportion of visible light to generate more photoinduced charge carriers.

Linear Sweep Voltammograms. Figure 5 shows the $J-V$ characteristics and current–time transient responses of the ZnO/ZnS, ZnO/ZnS/CdS, ZnO/ZnS/$CuInS_2$, ZnO/CdS/$CuInS_2$, and ZnO/ZnS/CdS/$CuInS_2$ nanowire arrays to evaluate their photoelectrochemical activity. Linear sweep voltammograms (LSV) were operated both in dark and under visible light irradiation. In the dark, all electrodes show tiny currents without observable difference. Therefore, only the current of the ZnO/ZnS electrode is illustrated (dash line in Figure 5A). As shown in Figure 5, under visible light illumination, the ZnO/ZnS nanowire array electrode exhibits very low photocurrent, whereas the photocurrents of other samples enhance obviously compared with the bare ZnO/ZnS electrode in the entire scanning region. It is due to the addition of visible light absorbers and the formation of heterostructure. At an applied potential of 0 V versus Ag/AgCl, the current density of ZnO/ZnS is 0.48 mA/cm^2. Under the same conditions, the current densities of the ZnO/ZnS/CdS,

dx.doi.org/10.1021/am501336u | ACS Appl. Mater. Interfaces 2014, 6, 8467–8474

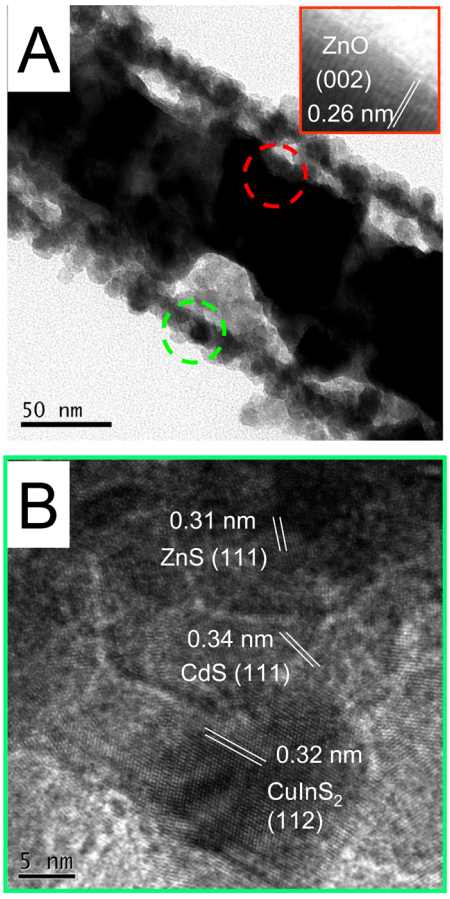

Figure 3. TEM (A) and HRTEM (B) images of ZnO/ZnS/CdS/$CuInS_2$. Inset is HRTEM image of ZnO.

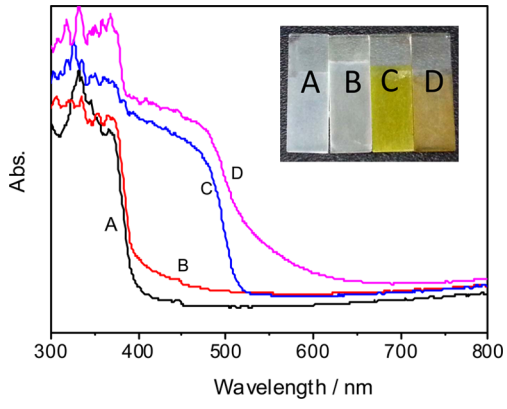

Figure 4. UV−vis spectra of (A) ZnO, (B) ZnO/ZnS, (C) ZnO/ZnS/CdS, and (D) ZnO/ZnS/CdS/$CuInS_2$ nanowire arrays. Insets are the optical images of corresponding samples.

ZnO/ZnS/$CuInS_2$, ZnO/CdS/$CuInS_2$, and ZnO/ZnS/CdS/$CuInS_2$ are 2.45, 0.96, 4.56, and 11.3 mA/cm^2, respectively. Moreover, the onset potential of ZnO/ZnS film is around −0.65 V, and the value shifts to −0.80 and −1.29 V after $CuInS_2$ and CdS are attached. The onset potentials of ZnO/CdS/$CuInS_2$ and ZnO/ZnS/CdS/$CuInS_2$ are about −1.32 and −1.35 V, respectively. The negative shift of onset potential indicates the decreased surface state densities of the electrodes and the increased charge transfer rates at the interfaces.[34,35]

***I*−*T* Curves.** The visible light responses of the ZnO/ZnS, ZnO/ZnS/CdS, ZnO/ZnS/$CuInS_2$, ZnO/CdS/$CuInS_2$, and

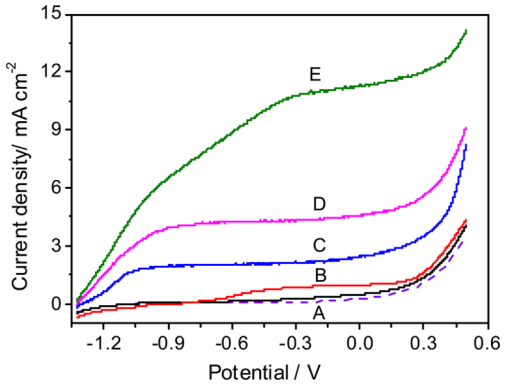

Figure 5. Current−potential curves of (A) ZnO/ZnS, (B) ZnO/ZnS/$CuInS_2$, (C) ZnO/ZnS/CdS, (D) ZnO/CdS/$CuInS_2$, and (E) ZnO/ZnS/CdS/$CuInS_2$ nanowire arrays in 0.50 M Na_2S/Na_2SO_3 solution. Scan rate: 100 mV/s.

ZnO/ZnS/CdS/$CuInS_2$ samples at an applied potential of 0 V versus Ag/AgCl are shown in Figure 6. As the light turns on,

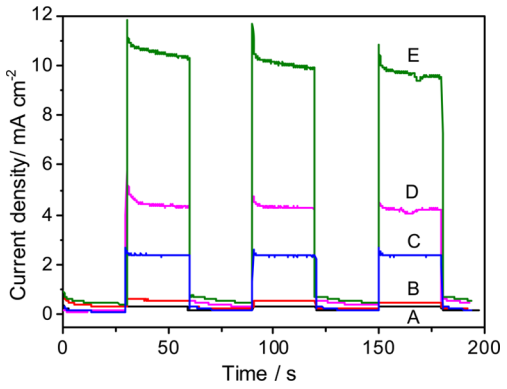

Figure 6. *I*−*T* curves of (A) ZnO/ZnS, (B) ZnO/ZnS/$CuInS_2$, (C) ZnO/ZnS/CdS, (D) ZnO/CdS/$CuInS_2$, and (E) ZnO/ZnS/CdS/$CuInS_2$ nanowire arrays in 0.50 M Na_2S/Na_2SO_3 solution, applied potential 0 V versus Ag/AgCl.

the photocurrent reaches a peak value and gradually decays to a steady state. A longer decay time is associated with a longer lifetime of photogenerated charge carriers.[24] In addition, Figure 6 clearly illustrates the photocurrent densities of the electrodes. A higher photocurrent corresponds to a higher efficiency of the PEC device of hydrogen evolution. The current density of the ZnO/ZnS electrode is 0.36 mA/cm^2. The loadings of CdS and $CuInS_2$ lead to notable increase in current density. The current densities of the ZnO/ZnS/CdS and ZnO/ZnS/CdS/$CuInS_2$ films are 2.40 and 10.5 mA/cm^2, respectively. The photocurrent of ZnO/ZnS/CdS/$CuInS_2$ is 29 times that of ZnO/ZnS and 4.4 times that of ZnO/ZnS/CdS. However, absence of either CdS or ZnS causes the decline of photoelectrochemical performance compared with ZnO/ZnS/CdS/$CuInS_2$. The photocurrent densities of ZnO/ZnS/$CuInS_2$ and ZnO/CdS/$CuInS_2$ are only 0.59 and 4.40 mA/cm^2, respectively, which are much lower than that of ZnO/ZnS/CdS/$CuInS_2$.

IPCE Measurement. To quantify the photoelectrochemical response of the samples to the incident light with various wavelengths, the IPCE measurements were performed on the sample electrodes at 0 V versus Ag/AgCl. The IPCE curves of the ZnO/ZnS, ZnO/ZnS/CdS, ZnO/ZnS/$CuInS_2$, ZnO/CdS/$CuInS_2$, and ZnO/ZnS/CdS/$CuInS_2$ films are presented in

dx.doi.org/10.1021/am501336u | ACS Appl. Mater. Interfaces 2014, 6, 8467−8474

Figure 7. The photoresponse of the ZnO/ZnS film is only active in the UV region. Upon the attachment of CdS, the

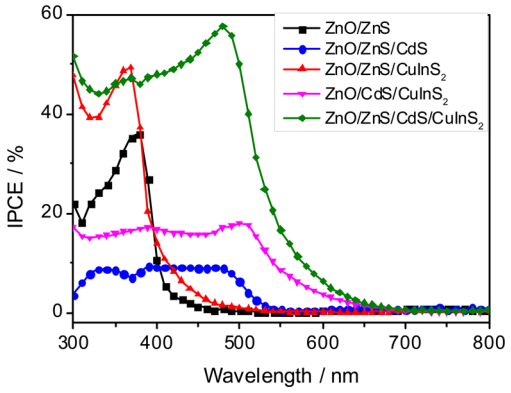

Figure 7. IPCE profiles of all samples collected at 0 V vs Ag/AgCl.

wavelength range of photoresponse extends to 530 nm, which is consistent with the absorption edge of ZnO/ZnS/CdS. Compared with the ZnO/ZnS/CdS film, the ZnO/ZnS/CdS/$CuInS_2$ film both extends wavelength coverage of photoresponse and increases IPCE values in the entire visible light region. The electrode exhibits the maximum IPCE of approximately 57.7% at 480 nm. The incorporation of $CuInS_2$ into ZnO/ZnS/CdS improves the electron-injection efficiency and also broadens the utilization range of the solar spectrum (i.e., the absorption edge shifts to the red light region). The improvement is mainly attributed to the p−n junctions formed between CdS and $CuInS_2$. However, in the absence of CdS or ZnS, the photoresponse of ZnO/ZnS/$CuInS_2$ and ZnO/CdS/$CuInS_2$ drops dramatically. In addition, ZnO/ZnS/$CuInS_2$ film only exhibits very low photocatalytic activity within the wavelength ranging from 400 to 450 nm, because ZnS and $CuInS_2$ cannot form efficient p−n junction due to their mismatched band alignment.[17]

Electrochemical Impedance Spectroscopy (EIS). Electrochemical impedance spectroscopy (Nyquist plots) was carried out to interpret the change of photocurrent and conversion efficiency of photon. Figure 8 shows electrochemical impedance spectra of composite nanowire arrays at AC frequency from 100 kHz to 1 Hz, which was performed under illumination at open circuit voltage. Charge transfer resistance (R_{ct}) from the photoelectrodes to redox species in

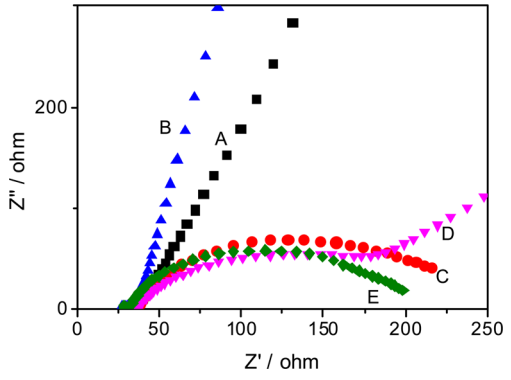

Figure 8. Electrochemical impedance spectra (Nyquist plots) of (A) ZnO/ZnS, (B) ZnO/ZnS/$CuInS_2$, (C) ZnO/ZnS/CdS, (D) ZnO/CdS/$CuInS_2$, and (E) ZnO/ZnS/CdS/$CuInS_2$ nanowire arrays.

the electrolyte can be calculated by fitting the semi-arc in the low frequency region.[17] Smaller circular radius represents lower electron transport resistance and higher separation efficiency of the photogenerated electrons and holes.[3] As can be seen from Figure 8, the R_{ct} of ZnO/ZnS and ZnO/ZnS/$CuInS_2$ is much larger than that of ZnO/ZnS/CdS, ZnO/CdS/$CuInS_2$, and ZnO/ZnS/CdS/$CuInS_2$, indicating much larger electron transport resistance and much poorer photoresponse, as curves A and B demonstrated in Figure 6. The R_{ct} of ZnO/ZnS/CdS/$CuInS_2$ is smaller than that of ZnO/CdS/$CuInS_2$ and ZnO/ZnS/$CuInS_2$, demonstrating that ZnS and CdS effectively restrain the recombination of photogenerated electrons and holes, thus the larger photocurrents are obtained. The matched potential positions of the valence band and conduction band of CdS with those of $CuInS_2$ result in the formation of effective p−n junction, which establishes an internal electrostatic field to promote the transportation of charge carriers and retards the recombination of electrons and holes in $CuInS_2$. Moreover, without ZnS layer, the electrons on the conduction band of ZnO would recombine with the electrolyte via the surface states or conduction band of $CuInS_2$, because their energy levels are close.[30] The surface states of ZnO can be effectively passivated by full covering of ZnS, and the recombination at the interface of the oxide and $CuInS_2$ is restrained. Thus, more charge carriers took part in the redox reactions.[30]

Mechanism. As mentioned above, the ZnO/ZnS/CdS/$CuInS_2$ core−shell nanowire array is proved to be one of the ideal structures for photoelectrochemical water splitting. Owing to nanowire-forest character, nanowire arrays provide effective electron percolation pathways, high surface-to-volume ratio for more reactive sites, and more effective harvest of the light. Moreover, the coarse surface reduces the reflection of incident light so as to increase the utilization of incident light.[15] In situ ion-exchange reaction ensures that high-quality heterojunctions form and reduces the surface defects of $CuInS_2$. Uniform core−shell structure with high-quality heterojunctions leads to efficient light absorption and effective separation of charge carriers. The ZnO/ZnS/CdS/$CuInS_2$ nanowire functions as follows: CdS and $CuInS_2$, direct narrow semiconductors with high absorption coefficient, act as excellent visible light captors to generate photoinduced charge carriers. ZnS, as a passivation layer, suppresses the recombination of electrons and holes at the interface of the oxide and $CuInS_2$, whereas ZnO acts as a pathway for the transportation of electrons. Furthermore, the p−n junction formed between CdS and $CuInS_2$ demonstrates a synergetic effect. The enhancement of the photoelectrical activity of ZnO/ZnS/CdS/$CuInS_2$ is higher than the sum of that of ZnO/ZnS/CdS and ZnO/ZnS/$CuInS_2$, indicating that the junction formed between $CuInS_2$ and CdS is favorable for electron transfer at the interface and for charge separation between $CuInS_2$ and CdS. Scheme 2 illustrates the photoinduced electron separation and transportation process in the ZnO/ZnS/CdS/$CuInS_2$ nanowire arrays. Under visible light illumination, photogenerated electrons in the conduction band of $CuInS_2$ flow to that of CdS, then to that of ZnO, and further to the counter electrode through external circuit to produce hydrogen. A stepwise conduction band edge limits the flux of electrons and reduces the recombination, leading to the enhancement of the performance.[17] Simultaneously, photogenerated holes in the valence band of the CdS transfer to that of $CuInS_2$, which react with the hole scavengers S^{2-} and SO_3^{2-} adhering to the $CuInS_2$ surface. Thus, the high photoelectrochemical activity of ZnO/ZnS/CdS/$CuInS_2$ is ascribed

Scheme 2. Photoinduced Electron Separation and Transportation Process in ZnO/ZnS/CdS/$CuInS_2$

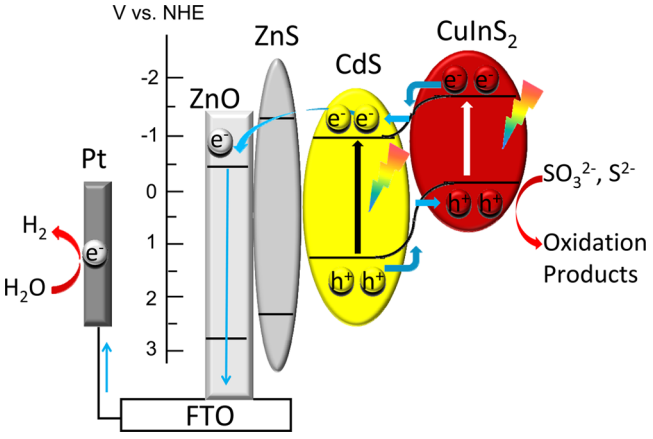

to the ZnS passivation layer and the intimate $CuInS_2$–CdS p–n heterojunction.

CONCLUSION

ZnO/ZnS/CdS/$CuInS_2$ core–shell nanowire arrays were fabricated via ion exchange and hydrothermal processes. The nanowires are perpendicularly aligned on FTO, with ZnO as a core wrapped with ZnS, CdS, and $CuInS_2$ multiple layers. The highest photocurrent of the ZnO/ZnS/CdS/$CuInS_2$ film reached 10.5 mA/cm^2 compared to 4.40 mA/cm^2 of the ZnO/CdS/$CuInS_2$ film and 0.59 mA/cm^2 of the ZnO/ZnS/$CuInS_2$ film. The IPCE of the ZnO/ZnS/CdS/$CuInS_2$ film was significantly enhanced in the entire visible light region by imposing ZnS and CdS. In such a configuration, ZnO acts as a pathway for electron transportation. $CuInS_2$ can capture a large proportion of visible light owing to its high absorption coefficient of 10^5 cm^{-1} and narrow direct bandgap (E_g) of 1.53 eV. ZnS, as a passivation layer, suppresses the recombination of electrons and holes at the interface of the oxide and $CuInS_2$. CdS also acts as an excellent visible light captor to generate photoinduced charge carriers. Moreover, the $CuInS_2$ is a p-type semiconductor when the atomic ratio of Cu to In exceeds 1. The intimate p–n junctions formed between $CuInS_2$ and CdS interfaces accelerate charge injection from one semiconductor to another, which leads to efficient charge separation and reduction of the recombination of electron–hole pairs by the internal electrostatic field in the interface. The above factors are supposed to be the main reasons for the generation of the enhanced photoelectrical response of the ZnO/ZnS/CdS/$CuInS_2$ system. The current work demonstrates that the core–shell configurations and heterostructures of ZnO/ZnS/CdS/$CuInS_2$ have great potential applications in the field of photoelectrical devices and photocatalysis for water splitting.

ASSOCIATED CONTENT

Supporting Information

Additional experimental details and results. This material is available free of charge via the Internet at http://pubs.acs.org/.

AUTHOR INFORMATION

Corresponding Author

*E-mail: (Y.X.Y.) yuyx@scut.edu.cn, (W.D.Z.) zhangwd@scut.edu.cn. Tel./Fax: 86-20-8711 4099.

Notes

The authors declare no competing financial interest.

ACKNOWLEDGMENTS

The authors thank the National Natural Science Foundation of China (nos. 21003051 and 21273080) for financial support.

REFERENCES

(1) Liu, R.; Lin, Y. J.; Chou, L. Y.; Sheehan, S. W.; He, W. S.; Zhang, F.; Hou, H. J. M.; Wang, D. W. Water Splitting by Tungsten Oxide Prepared by Atomic Layer Deposition and Decorated with an Oxygen-Evolving Catalyst. *Angew. Chem., Int. Ed.* **2011**, *50*, 499–502.

(2) Zhang, K.; Guo, L. J. Metal Sulphide Semiconductors for Photocatalytic Hydrogen Production. *Catal. Sci. Technol.* **2013**, *3*, 1672–1690.

(3) Liu, Y.; Wang, D. P.; Yu, Y. X.; Zhang, W. D. Preparation and Photoelectrochemical Properties of Functional Carbon Nanotubes and Ti Co-Doped Fe_2O_3 Thin Films. *Int. J. Hydrogen Energy* **2012**, *37*, 9566–9575.

(4) Li, Y.; Zhang, J. Z. Hydrogen Generation from Photoelectrochemical Water Splitting Based on Nanomaterials. *Laser Photonics Rev.* **2010**, *4*, 517–528.

(5) Lin, Y. J.; Yuan, G. B.; Liu, R.; Zhou, S.; Sheehan, S. W.; Wang, D. W. Semiconductor Nanostructure-Based Photoelectrochemical Water Splitting: A Brief Review. *Chem. Phys. Lett.* **2011**, *507*, 209–215.

(6) Szymanski, P.; El-Sayed, M. A. Some Recent Developments in Photoelectrochemical Water Splitting using Nanostructured TiO_2: A Short Review. *Theor. Chem. Acc.* **2012**, *131*, 1202.

(7) Paracchino, A.; Mathews, N.; Hisatomi, T.; Stefik, M.; Tilley, S. D.; Gratzel, M. Ultrathin Films on Copper(I) Oxide Water Splitting Photocathodes: A Study on Performance and Stability. *Energy Environ. Sci.* **2012**, *5*, 8673–8681.

(8) Hou, Y.; Zuo, F.; Dagg, A.; Feng, P. Y. Visible Light-Driven alpha-Fe_2O_3 Nanorod/Graphene/$BiV_{1-x}Mo_xO_4$ Core/Shell Heterojunction Array for Efficient Photoelectrochemical Water Splitting. *Nano Lett.* **2012**, *12*, 6464–6473.

(9) Kim, J.; Minegishi, T.; Kobota, J.; Domen, K. Enhanced Photoelectrochemical Properties of $CuGa_3Se_5$ Thin Films for Water Splitting by the Hydrogen Mediated Co-Evaporation Method. *Energy Environ. Sci.* **2012**, *5*, 6368–6374.

(10) Zhang, W. D.; Jiang, L. C.; Ye, J. S. Photoelectrochemical Study on Charge Transfer Properties of ZnO Nanowires Promoted by Carbon Nanotubes. *J. Phys. Chem. C* **2009**, *113*, 16247–16253.

(11) Xie, S. L.; Lu, X. H.; Zhai, T.; Li, W.; Yu, M. H.; Liang, C. L.; Tong, Y. X. Enhanced Photoactivity and Stability of Carbon and Nitrogen Co-Treated ZnO Nanorod Arrays for Photoelectrochemical Water Splitting. *J. Mater. Chem.* **2012**, *22*, 14272–14275.

(12) Law, M.; Greene, L. E.; Johnson, J. C.; Saykally, R.; Yang, P. D. Nanowire Dye-Sensitized Solar Cells. *Nat. Mater.* **2005**, *4*, 455–459.

(13) Jiang, L. C.; Zhang, W. D.; Yu, Y. X.; Wang, J. Preparation and Charge Transfer Properties of Carbon Nanotubes Supported CdS/ZnO–NWs Shell/Core Heterojunction. *Electrochem. Commun.* **2011**, *13*, 627–630.

(14) Zhong, M.; Li, Y. B.; Yamada, I.; Delaunay, J. J. ZnO-$ZnGa_2O_4$ Core–Shell Nanowire Array for Stable Photoelectrochemical Water Splitting. *Nanoscale* **2012**, *4*, 1509–1514.

(15) Li, Y. B.; Liu, Z. F.; Wang, Y.; Liu, Z. C.; Han, J. H.; Ya, J. ZnO/$CuInS_2$ Core/Shell Heterojunction Nanoarray for Photoelectrochemical Water Splitting. *Int. J. Hydrogen Energy* **2012**, *37*, 15029–15037.

(16) Lin, Y. G.; Hsu, Y. K.; Chen, Y. C.; Wang, S. B.; Miller, J. T.; Chen, L. C.; Chen, K. H. Plasmonic Ag@Ag-3(PO4)(1–*x*) Nanoparticle Photosensitized ZnO Nanorod-Array Photoanodes for Water Oxidation. *Energy Environ. Sci.* **2012**, *5*, 8917–8922.

(17) Xu, G. P.; Ji, S. L.; Miao, C. H.; Liu, G. D.; Ye, C. H. Effect of ZnS and CdS Coating on the Photovoltaic Properties of $CuInS_2$-Sensitized Photoelectrodes. *J. Mater. Chem.* **2012**, *22*, 4890–4896.

(18) Ikeda, S.; Nakamura, T.; Lee, S. M.; Yagi, T.; Harada, T.; Minegishi, T.; Matsumura, M. Photoreduction of Water by using Modified $CuInS_2$ Electrodes. *ChemSusChem* **2011**, *4*, 262−268.
(19) Xia, J.; Liu, Y.; Qiu, X. B.; Mao, Y. C.; He, J. S.; Chen, L. P. Solvothermal Synthesis of Nanostructured $CuInS_2$ Thin Films on FTO Substrates and their Photoelectrochemical Properties. *Mater. Chem. Phys.* **2012**, *136*, 823−830.
(20) Das, K.; Panda, S. K.; Gorai, S.; Mishra, P.; Chaudhuri, S. Effect of Cu/In Molar Ratio on the Microstructural and Optical Properties of Microcrystalline $CuInS_2$ Prepared by Solvothermal Route. *Mater. Res. Bull.* **2008**, *43*, 2742−2750.
(21) Zheng, J. Y.; Song, G.; Kim, C. W.; Kang, Y. S. Facile Preparation of p-CuO and p-CuO/n-$CuWO_4$ Junction Thin Films and their Photoelectrochemical Properties. *Electrochim. Acta* **2012**, *69*, 340−344.
(22) Liu, Y.; Yu, Y. X.; Zhang, W. D. MoS_2/CdS Heterojunction with High Photoelectrochemical Activity for H-2 Evolution under Visible Light: The Role of MoS_2. *J. Phys. Chem. C* **2013**, *117*, 12949−12957.
(23) Li, J. T.; Meng, F. K.; Suri, S.; Ding, W. Q.; Huang, F. Q.; Wu, N. Q. Photoelectrochemical Performance Enhanced by a Nickel Oxide-Hematite p−n Junction Photoanode. *Chem. Commun.* **2012**, *48*, 8213−8215.
(24) Dai, G. P.; Yu, J. G.; Liu, G. Synthesis and Enhanced Visible-Light Photoelectrocatalytic Activity of p−n Junction BiOI/TiO_2 Nanotube Arrays. *J. Phys. Chem. C* **2011**, *115*, 7339−7346.
(25) Yun, J. H.; Ng, Y. H.; Huang, S. J.; Conibeer, G.; Amal, R. Wrapping the Walls of n-TiO_2 Nanotubes with p-$CuInS_2$ Nanoparticles using Pulsed-Electrodeposition for Improved Heterojunction Photoelectrodes. *Chem. Commun.* **2011**, *47*, 11288−11290.
(26) Lee, D.; Yong, K. Superstrate $CuInS_2$ Photovoltaics with Enhanced Performance Using a CdS/ZnO Nanorod Array. *ACS Appl. Mater. Interfaces* **2012**, *4*, 6757−6764.
(27) Wang, Y. Q.; Rui, Y. C.; Zhang, Q. H.; Li, Y. G.; Wang, H. Z. A Facile in Situ Synthesis Route for $CuInS_2$ Quantum-Dots/In_2S_3 Co-Sensitized Photoanodes with High Photoelectric Performance. *ACS Appl. Mater. Interfaces* **2013**, *5*, 11858−11864.
(28) Luo, J. H.; Wei, H. Y.; Huang, Q. L.; Hu, X.; Zhao, H. F.; Yu, R. C.; Li, D. M.; Luo, Y. H.; Meng, Q. B. Highly Efficient Core-Shell $CuInS_2$-Mn Doped CdS Quantum Dot Sensitized Solar Cells. *Chem. Commun.* **2013**, *49*, 3881−3883.
(29) Kuo, K. T.; Liu, D. M.; Chen, S. Y.; Lin, C. C. Core−Shell $CuInS_2$/ZnS Quantum Dots Assembled on Short ZnO Nanowires with Enhanced Photo-Conversion Efficiency. *J. Mater. Chem.* **2009**, *19*, 6780−6788.
(30) Guijarro, N.; Campina, J. M.; Shen, Q.; Toyoda, T.; Lana-Villarreal, T.; Gomez, R. Uncovering the Role of the ZnS Treatment in the Performance of Quantum Dot Sensitized Solar Cells. *Phys. Chem. Chem. Phys.* **2011**, *13*, 12024−12032.
(31) Chen, C.; Ali, G.; Yoo, S. H.; Kum, J. M.; Cho, S. O. Improved Conversion Efficiency of CdS Quantum Dot-Sensitized TiO_2 Nanotube-Arrays using $CuInS_2$ as a Co-Sensitizer and an Energy Barrier Layer. *J. Mater. Chem.* **2011**, *21*, 16430−16435.
(32) Li, T. L.; Lee, Y. L.; Teng, H. S. $CuInS_2$ Quantum Dots Coated with CdS as High-Performance Sensitizers for TiO_2 Electrodes in Photoelectrochemical Cells. *J. Mater. Chem.* **2011**, *21*, 5089−5098.
(33) Xu, C. K.; Shin, P.; Cao, L. L.; Gao, D. Preferential Growth of Long ZnO Nanowire Array and Its Application in Dye-Sensitized Solar Cells. *J. Phys. Chem. C* **2010**, *114*, 125−129.
(34) Yoon, K. H.; Shin, C. W.; Kang, D. H. Photoelectrochemical Conversion in a WO_3 Coated p-Si Photoelectrode: Effect of Annealing Temperature. *J. Appl. Phys.* **1997**, *81*, 7024−7029.
(35) Yoon, K. H.; Seo, D. K.; Cho, Y. S.; Kang, D. H. Effect of Pt Layers on the Photoelectrochemical Properties of a WO_3/p-Si Electrode. *J. Appl. Phys.* **1998**, *84*, 3954−3959.